Magnesium Sheet Alloy Development for Room Temperature Forming

Alan A. Luo*, Renhai Shi, Jiashi Miao, Thomas Avey
The Ohio State University, Columbus, OH, USA

Abstract

Sheet metal forming operations in the automotive industry, including stamping, flanging, bending, hemming and trimming, are dominantly done at room temperature (RT). Unfortunately, the poor RT formability of magnesium due to its hexagonal close packed (HCP) structure and generally strong texture has limited the use of these processes in high-volume automotive production. However, the formability of magnesium can be improved via fine grain structure and random texture to enable some RT forming operations. This paper presents the latest magnesium alloy development and evaluation by the United States Automotive Materials Partnership (USAMP) in collaboration with its university partners. A new sheet alloy developed in a recent USAMP project, ZAXME11100 (USAMP Alloy 2 Plus), offers excellent ductility (31% tensile elongation) and RT formability (7.8 mm Erichsen Index) in solution-treated condition (T4), and a high yield strength (270 MPa) upon post-forming aging treatment (T6), promising RT forming for automotive applications.

*Corresponding author: A.A. Luo (luo.445@osu.edu)

INTRODUCTION

Reducing vehicle weight is an important approach for increasing fuel economy, addressing regulatory requirements, and meeting consumer needs [1]. Lightweight materials have played an important role in reducing the mass and improving the fuel economy of automobiles over the last 50 years [2]. Magnesium, the lightest structural metal [3], has been a subject of research from almost the beginning of the United States Automotive Materials Partnership (USAMP), established in 1993 between FiatChrysler, Ford and General Motors to share the risk for developing advanced lightweighting technologies. Since its inception, USAMP has collaborated extensively with the U.S. Department of Energy (DOE) to conduct research and development aimed at reducing the mass of automobiles though strategic use of lightweight materials. Early magnesium projects at USAMP had focused on casting applications in interior, powertrain and chassis components [4], primarily due to the excellent castability of magnesium alloys and part consolidation and high productivity opportunities offered by high pressure die casting processes [5].

As magnesium is making inroads into more critical applications in chassis and body areas, there is an urgent need for developing wrought magnesium products and manufacturing processes to provide improved mechanical properties, formability and corrosion resistance [6]. Therefore, wrought magnesium alloys have been evaluated for sheet and extrusion applications in a number of USAMP projects. The first USAMP project involving sheet magnesium alloys was "Magnesium Front End Research and Development" started in 2007 [7], where the most commonly used AZ31B (Mg-3Al-1Zn[1]) sheet alloy was evaluated for formability and crashworthiness in automotive conditions. When compared to steel or aluminum sheet alloys used in the automotive industry, AZ31B-H24 showed limited formability at room temperature due to its hexagonal close packed (HCP) crystal structure [4], and poor crashworthiness due to its unfavorable fracture behavior under crash loading conditions [7]. Later, a follow on USAMP project [8, 9] designed, built and tested a "demonstration" structure, as shown in Figure 1 [8], which included an upper rail made with AZ31B sheet by warm-forming to overcome the limited room temperature formability of magnesium. These projects provided important material property databases and enabling processing (including joining) technologies for design and manufacturing sheet magnesium applications.

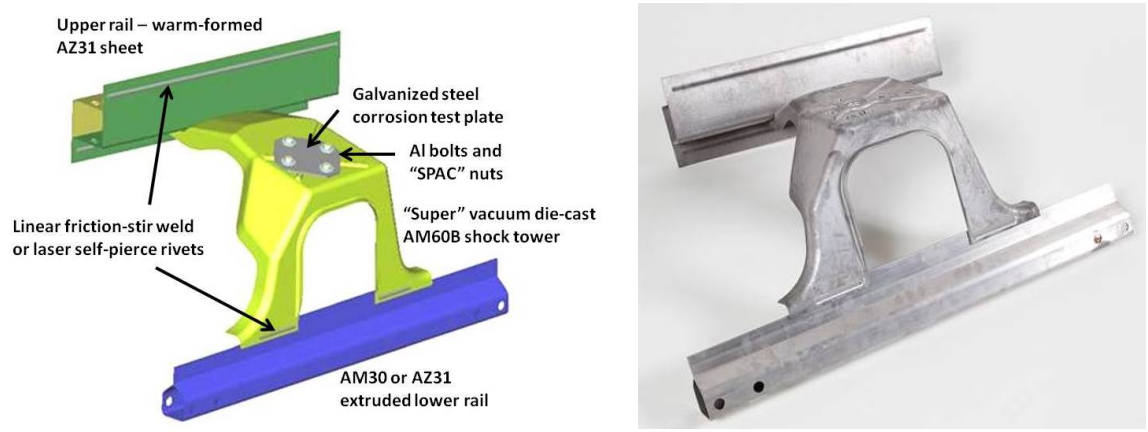

(a) Design (b) Build

Figure 1. USAMP magnesium-intensive front-end "demonstration" structure including an upper rail made of AZ31B sheet by warm-forming: (a) design; and (b) build.

[1] All concentrations in weight percentage.

Sheet metal forming operations in the automotive industry, including stamping, flanging, bending, hemming and trimming, are dominantly done at room temperature. The processes are very robust with the common higher formability materials such as steels and aluminum. Unfortunately, the limited formability of magnesium makes the use of these processes very challenging, which has been demonstrated in two of the USAMP projects on warm forming of aluminum and magnesium sheet alloys [10, 11]. Figure 2 compares results of room temperature forming using a simple rectangular pan for mild steel and AZ31B-H24 magnesium sheet. The pan could be formed to a depth of 125 mm with steel but split after only about 12 mm with the magnesium [10]. Thus, magnesium sheet is generally formed at elevated temperature forming processes, which are considerably more expensive than room temperature forming. To this date, the automotive use of magnesium sheet in North America is virtually non-existent, with only limited low-volume production applications (using various elevated temperature forming techniques) in Europe and Korea, such as the center console and roof panel for the Porsche Carrera GT and luggage retainer for Renault-Samsung SM7.

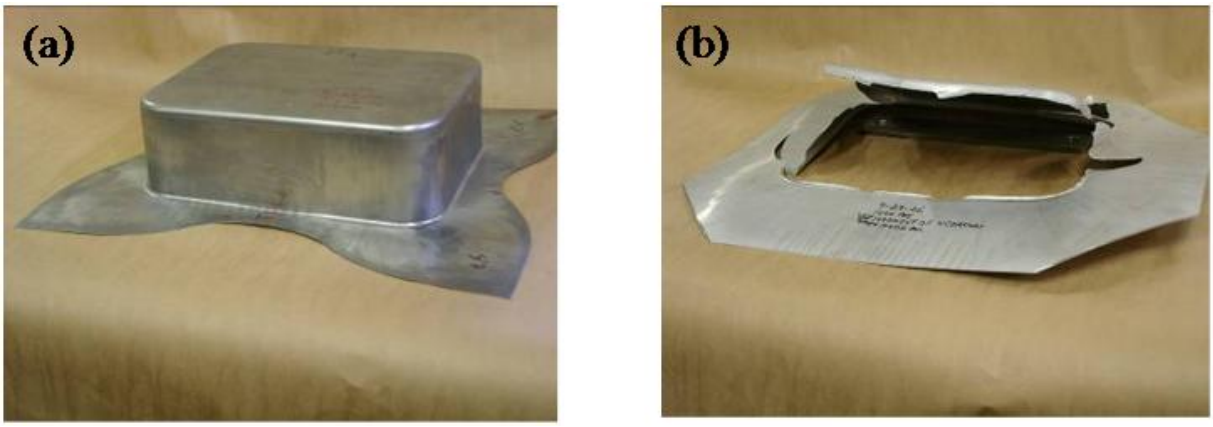

Figure 2. Comparison of a forming trial on a 125 mm deep pan with (a) mild steel and (b) AZ31B-H24 magnesium sheet (reprinted from ref. 4 with permission).

Based on the above research, it is clear that the room-temperature formability of current magnesium alloys such as AZ31B does not meet the automotive requirements in cost and performance for high-volume production. In 2016, USAMP was awarded a project by DOE, *Low-Cost Magnesium Sheet Component Development and Demonstration Project*, to demonstrate the feasibility of producing magnesium sheet components at affordable costs. To achieve this goal, the USAMP team is collaborating with several suppliers, universities, and national labs to research, develop, test, and evaluate at least one magnesium alloy and commensurate processing configuration suitable for rolling thin, automotive appearance grade sheet, and forming large, challenging automotive panels. This paper will summarize the work carried out at The Ohio State University in the last three years, as a part of the USAMP project, to design and develop a new magnesium alloy with improved formability at room temperature.

BASELINE ALLOYS

AZ31B

Commercial alloy AZ31B is commercially available in either an annealed, O temper, or in a partially-annealed, H24 temper. Typical microstructure of AZ31B in these two temper conditions is shown in Figure 3 [4].

Figure 3(a, b) shows that the annealed (O temper) material has a generally homogeneous distribution of grains with clearly visible boundaries, while the as rolled (H24 temper) material in Figure 3(c) is highly worked with no clear grain boundaries. In the O temper, the AZ31 material has similar yield strength to work-hardenable aluminum sheet alloys such as AA5754 or AA5182, but lower strength than age-hardenable alloys such as AA6111. One issue with sheet magnesium is that the properties are typically anisotropic, i.e., the strength or ductility varies with direction on the sheet. For example, yield strength of AZ31B alloy is typically approximately 10% lower transverse to the rolling direction compared with parallel to the rolling direction [4]. The anisotropy has been attributed to, (i) irregular or non-homogeneous grains and (ii) texture differences, between the rolling and transverse to rolling directions. An example of grain inhomogeneity is shown in Figure 3(c), which shows regions of very fine grains oriented in bands (indicated by an arrow) through the material.

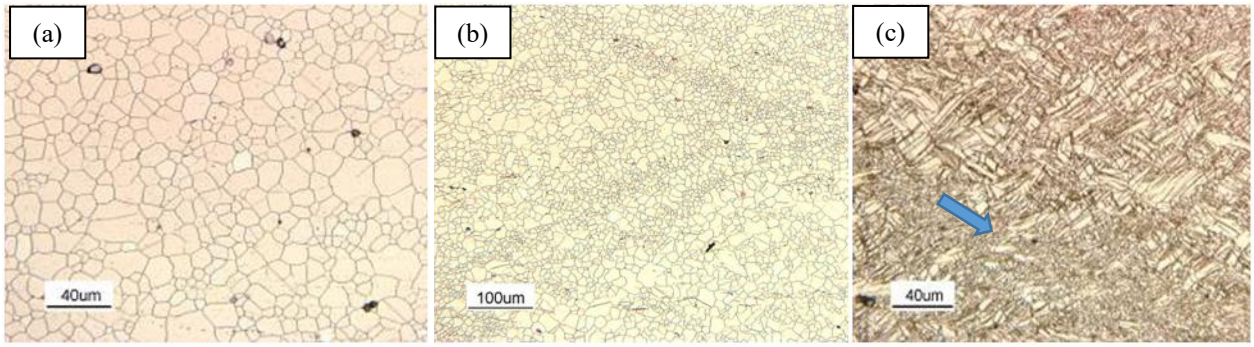

Figure 3. Typical microstructures in AZ31 sheet showing (a, b) fully annealed, O temper; and (c) partially annealed, H24 temper (arrow indicates slip bands) (adapted from ref. 4 with permission).

Another issue with AZ31B sheet alloy is its strong tension-compression asymmetry shown in Figure 4 [12]; about 25% difference in tensile and compressive yield strengths and significantly different hardening/softening behaviors in tension and compression, which makes the design and CAE (computer-aided engineering) analyses of this material very challenging. A USAMP team [13] took on the challenge and developed a new material model using the MAT_124 card in LS-DYNA, incorporating both the tension-compression asymmetry and the strain rate dependency of AZ31B sheet. This model has been validated in four-point quasi-static bending and axial compression tests (both slow and fast speeds) on a rivet-bonded double top hat beam using AZ31B sheet (Figure 5). Using the MAT_124 material card coupled with strain-based element deletion, LS-DYNA analyses accurately captured the material behavior in these three loading conditions [13]. Figure 5 also shows fragmented fracture behavior of AZ31B beams in high-speed sled axial crush tests, which is not desirable for automotive applications on critical crash load paths. Similar behavior was also reported by the USAMP team [14] for test beams made from AM60B (Mg-6Al-0.4Mn) die castings and AM30 (Mg-3Al-0.4Mn) extrusions. While the exact reason for this less than desirable fracture behavior under high strain rates is still a subject of research, it is clear that it is related to the deformation mechanisms of magnesium alloys.

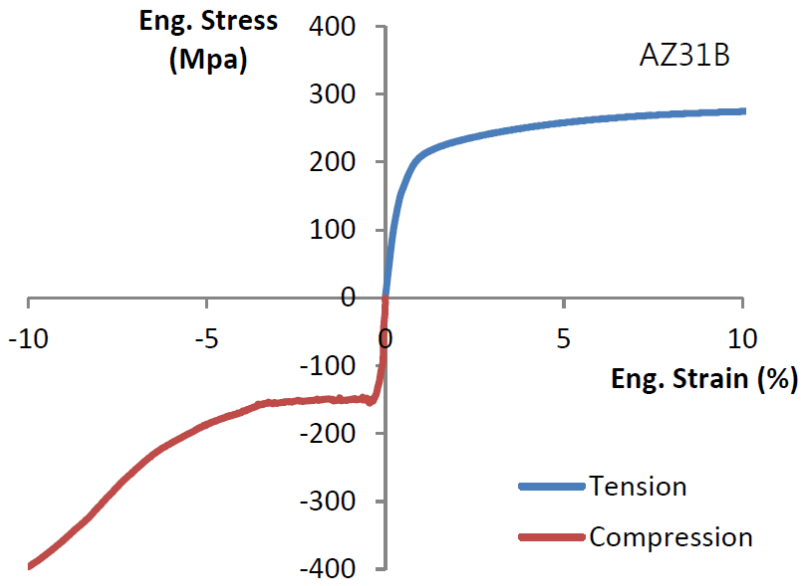

Figure 4. Tension-compression asymmetry in AZ31B sheet material (courtesy of Posco [12]).

(a) FEA prediction (b) Physical test results

Figure 5. High-speed sled axial crush test of double top hat beams of AZ31B sheet magnesium: (a) FEA prediction, and (b, c) physical test results (reprinted from ref. 13 with permission).

Recent Alloy Development

Recent research has shown that the mechanical behavior of magnesium alloys can be improved via tailoring the magnesium matrix with addition of alloying elements [15-17] and thermomechanical processing [18, 19]. Alloying elements (such as Al, Zn, Ca, Mn, and rare-earth elements) have been shown to significantly improve the mechanical properties of magnesium alloys at room temperature. Additions of zinc (Zn), calcium (Ca), and manganese (Mn) can improve the strength of magnesium alloys via solid solution strengthening [20], precipitation strengthening [21-23], and grain boundary strengthening [22]. Grain refinement strengthening [24] can improve ductility or formability via weakening of the strong basal texture of magnesium alloys [23, 25-27]. Trace additions of rare-earth elements such as yttrium (Y), neodymium (Nd), and cerium (Ce) can improve the strength and ductility of magnesium alloys. The improvement could be attributed to reduced intrinsic stacking fault I1 energy (I1 SFE) [28] to generate <c+a> dislocations, lower critical resolved shear stress (CRSS) of pyramidal <c+a>slip [29], and more randomized texture [20].

Among the many experimental magnesium sheet alloys reported around the world, the following two were available for evaluation by the USAMP team in collaboration with their university partners.

ZEK100 Alloy

ZEK100 (Mg-1.2Zn-0.17Nd-0.35Zr) is a rare-earth containing magnesium sheet alloy commercially available as Elektron 717 [32]. Figures 6 and 7 show the tension and compression responses at room temperature of ZEK100 (O temper, annealed at 450°C for 1 h and then furnace cooled to RT) and AZ31B (O temper, annealed at 350°C for 1 h and then air cooled to RT), respectively, with the corresponding 0.2% offset yield stresses summarized in Table 1 [33]. These results suggest that, irrespective of the loading type (i.e. tension or compression), ZEK100 sheet specimens (1.6 mm thick) exhibited lower flow stresses and higher ductility compared with AZ31B alloy. Additionally, the tension-compression yield stress asymmetry ratios (Table 2 [33]) are considerably lower for ZEK100 compared with AZ31B sheet specimens, but slightly more pronounced planar anisotropy for ZEK100 alloy between RD and TD directions, i.e., $(\sigma_{TD}/\sigma_{RD})_{tension} = 0.56$.

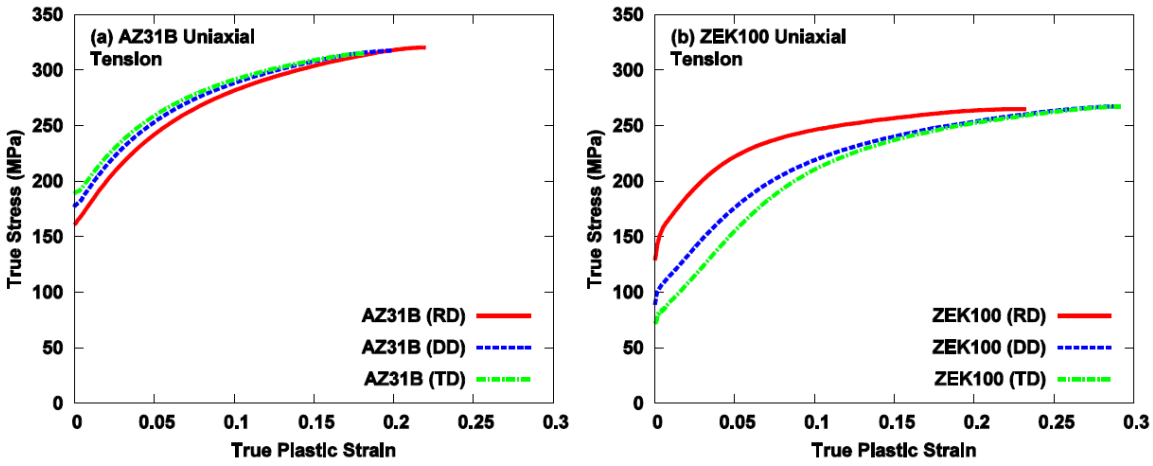

Figure 6. True stress vs. true plastic strain response under tension for (a) AZ31B; and (b) ZEK100 (reprinted from ref. 33 with permission).

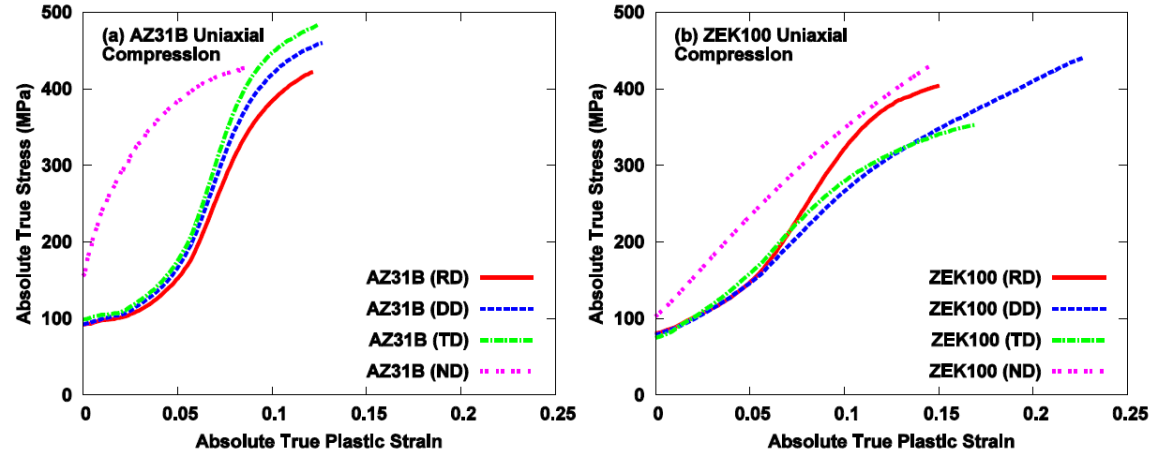

Figure 7. True stress vs. true plastic strain response under compression for (a) AZ31B; and (b) ZEK100 (reprinted from ref. 33 with permission).

Table 1. 0.2% offset yield stresses under tension and compression for AZ31B and ZEK100 (adapted from ref. 33 with permission).

		RD	DD	TD	ND
AZ31B	$\sigma_{0.2\%}^{tension}(MPa)$	161	177	189	-
	$\sigma_{0.2\%}^{compression}(MPa)$	92	93	99	156
ZEK100	$\sigma_{0.2\%}^{tension}(MPa)$	129	89	72	-
	$\sigma_{0.2\%}^{compression}(MPa)$	81	79	75	103

Table 2. Yield stress asymmetry and anisotropy ratios for AZ31 and ZEK100 sheet specimens (adapted from ref. 33 with permission).

Yield stress asymmetry ratio ($\sigma_{tension}/\sigma_{compression}$)				Yield stress anisotropy ratio
	RD	DD	TD	
AZ31B	1.75	1.90	1.91	$(\sigma_{TD}/\sigma_{RD})_{tension} = 1.17$ $(\sigma_{TD}/\sigma_{RD})_{compression} = 1.07$
ZEK100	1.59	1.13	0.96	$(\sigma_{TD}/\sigma_{RD})_{tension} = 0.56$ $(\sigma_{TD}/\sigma_{RD})_{compression} = 0.93$

The measured texture corresponding to annealed AZ31B and annealed ZEK100 sheets are shown in Figures 8 and 9, respectively. For AZ31B, a strong initial basal texture is evident in its inverse pole figure (Figure 8(a)) and is consistent with the {0001} basal pole figure (Figure 8(b)), showing the majority of c-axes aligned normal to the sheet plane. However, there is a spreading of the basal poles towards RD, as evidenced by an ellipsoidal intensity distribution of the {0001} pole figure. For ZEK100 sheet, the IPF map (Figure 9(a)) shows grains of several different colors distributed more randomly, indicating a relatively weak basal texture for ZEK100 (Figure 9(b)), with significant spreading of basal poles along TD and a weaker peak intensity as compared with that of AZ31B sheet.

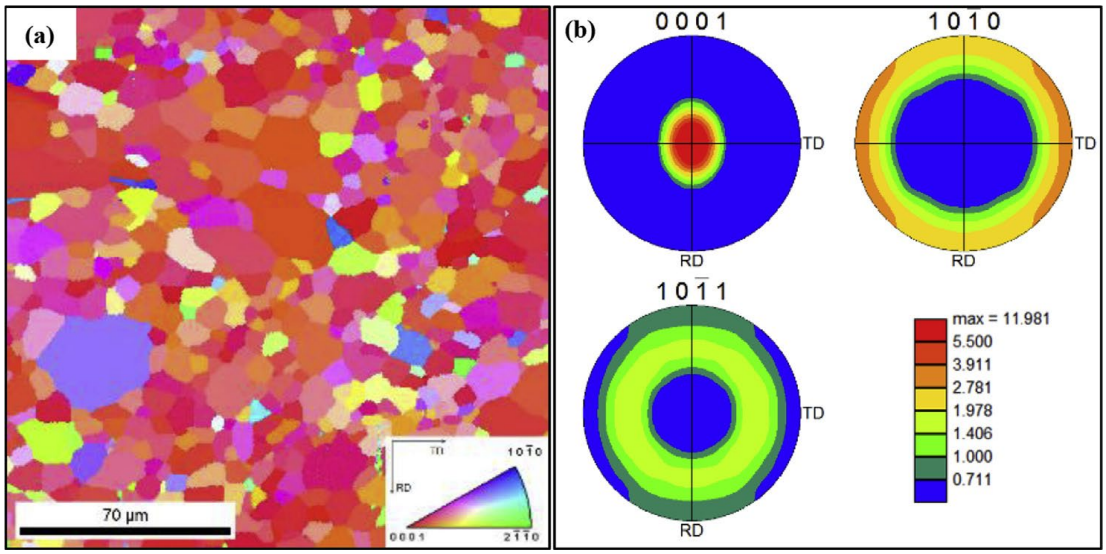

Figure 8. (a) Initial texture and (b) pole figures for annealed AZ31B-O sheet. The RD-TD plane represents the rolled surface of the sheet (reprinted from ref. 33 with permission).

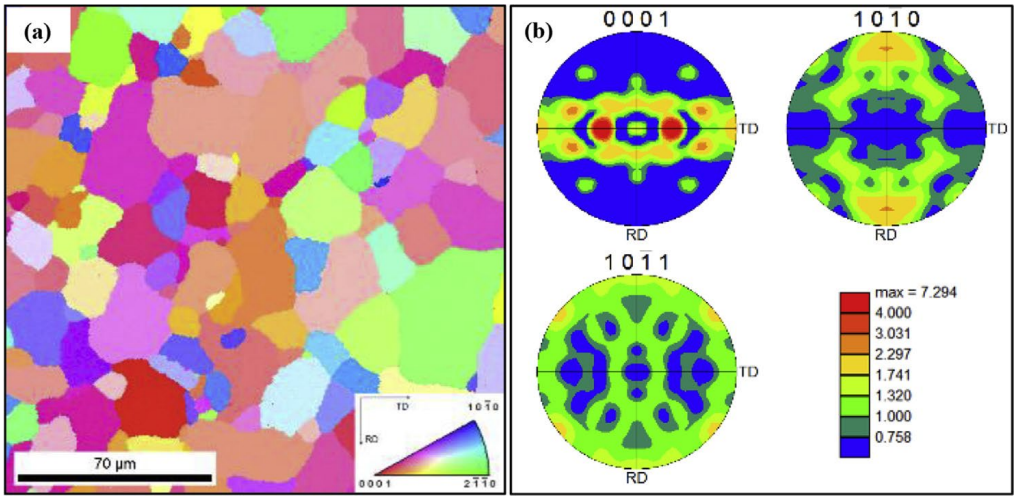

Figure 9. (a) Initial texture and (b) pole figures for annealed ZEK100 sheet. The RD-TD plane represents the rolled surface of the sheet (reprinted from ref. 33 with permission).

Overall, ZEK100 alloy shows improved ductility (but reduced yield strength) and less tension-compression asymmetry, due to the more random and weaker texture, compared to AZ31B sheet alloy. However, the formability of ZEK100 has not significantly improved to the level of room-temperature forming. It is, therefore, recommended [32] that the alloy be formed using room temperature dies with material temperatures around 215°C (420°F). It can also be superplastically formed at higher temperatures, and warm hemmed at temperatures as low as 120°C (248°F).

E-Form Alloys

E-Form, meaning *easy and economically formable*, is the name of POSCO's new proprietary magnesium sheet alloys. Although the exact chemical compositions of E-Form and E-Form Plus grades are held proprietary by POSCO, it has been reported that they are essentially Ca-modified AZ31 [34]. Table 3 summarizes the tensile properties and bendability of E-Form alloys compared with AZ31B from POSCO (R: bend radius; t: sheet thickness 1.2 mm) E-Form [35]. Figure 10 shows that a 0.5%Ca addition can significantly enhance the formability of the AZ31B alloy, with the Erichsen value increased from 2.2 mm to 6 mm [34]. Figure 11 shows the EBSD results including normal direction (ND) IPF maps, image quality (IQ) maps, and grain size distribution of AZ31 and AZ31-0.5Ca alloys.

Table 3. Tensile properties and bendability of E-From alloys in comparison with AZ31B from POSCO (R: bend radius; t: sheet thickness 1.2 mm) E-Form (courtesy of Posco [35]).

Alloy	Direction	YS (MPa)	El. (%)	Limit Bending Radius/Thickness Ratio (R/t)			
		Room temperature		RT	150 °C	200 °C	250 °C
E-Form Plus	RD	169	25.0	2.3	1.2	0.1	0
	TD	142	21.0	3.1	2.8	1.5	0.9
E-Form	RD	151	27.3	2.1	1.4	0.7	0.4
	TD	144	15.4	4.3	3.2	2.9	2.9
AZ31	RD	177	28.5	8.0	2.3	1.8	1.4
	TD	209	24.3	7.5	3.6	2.3	1.8

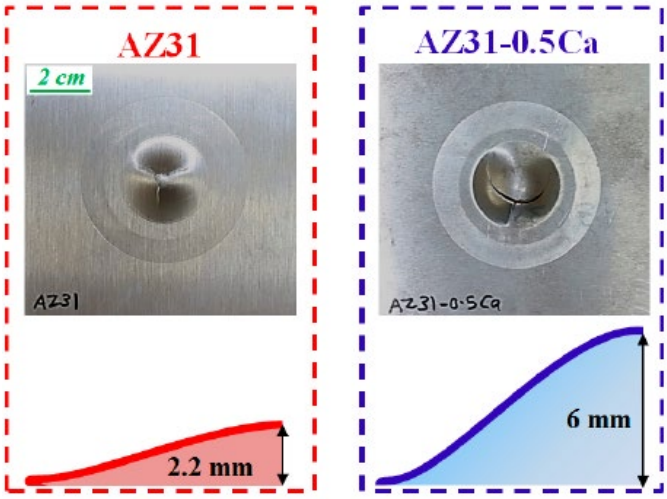

Figure 10. Top views and profiles taken from the AZ31B and AZ31B-0.5Ca alloy sheets after Erichsen test (reprinted from ref. 34, under the terms of the Creative Commons CC BY license).

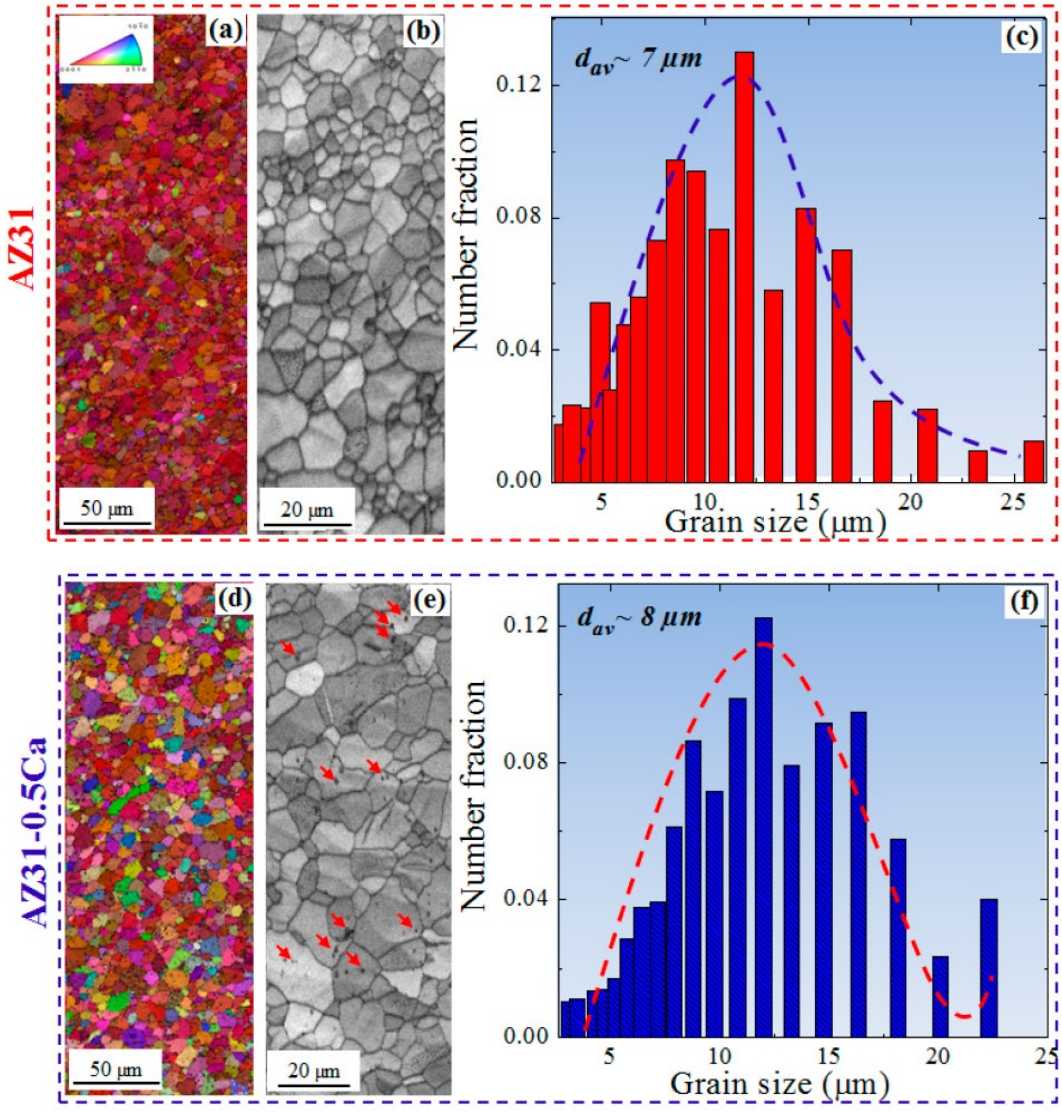

Figure 11. (a, d) ND inverse pole figure maps; (b, e) image quality maps; and (c, f) grain size distribution of AZ31 and AZ31-0.5Ca alloys, respectively. The grain size measurements by EBSD experiment were conducted at a tolerance angle of 2° (reprinted from ref. 34, under the terms of the Creative Commons CC BY license).

This improved formability of the AZ31-0.5Ca alloy (Figure 10) was attributed to the role of the Ca addition in weakening the basal texture (Figure 11), resulting in lower plastic anisotropy shown by tensile tests in three-directions [34]. Viscoplastic self-consistent (VPSC) modeling was used to predict the critical resolved shear stress (CRSS) of basal and non-basal slip systems in these two alloys [36]. The results showed that the addition of 0.5% Ca enhanced the activity of prismatic <a> slip, leading to higher ductility in this alloy (AZ31-0.5Ca). With improved formability, E-Form alloy has been used in laptop cases for LG Gram 15Z960 and Samsung Notebook 9 NT900X3L [35]. However, the E-Form alloys haven't been reported to be in use in automotive mass production.

USAMP ALLOY DEVELOPMENT

While the USAMP team is evaluating the ZEK100 and E-Form Plus sheet alloys for low-cost automotive applications, The Ohio State University (OSU) is tasked in a parallel path to develop new magnesium sheet alloys with further improved formability. This section summarizes the two experimental alloys designed by the OSU team, promising room-temperature formability.

ZXEM2000 (USAMP Alloy 2)

The recent alloy development work has shown that alloying is an effective way to modify the microstructure and improve the mechanical properties of magnesium alloys. Based on CALculation of Phase Diagram (CALPHAD) modeling [30, 31] approach, Mg-2Zn-0.3Ca-0.2Ce-0.1Mn (designated as ZXEM2000 alloy, also called USAMP Alloy 2), is designed to offer more balanced strength and ductility [37]. Thermomechanical processing (TMP), including homogenization, rolling and annealing, is critical to maximizing the alloying effects for final mechanical properties. Conventional homogenization processes (at temperatures below the alloy's solidus to avoid incipient melting) are inefficient in maximizing solute concentrations in the Mg matrix since the low diffusivities of the alloying elements cannot completely dissolve secondary phases from the as-cast microstructure at these low temperatures. CALPHAD simulation was used to design a new homogenization process (multiple isothermal stages with final stages at temperatures higher than the alloy's solidus) for the new alloy, to achieve complete dissolution of the alloying elements without incipient melting. The combination of the new alloy design and TMP process provides an excellent combination of strength and ductility at room temperature for USAMP Alloy 2.

Figure 12(a) is calculated solidification path of USAMP Alloy 2, based on the classical Scheil model. It shows that primary Mg phase will form at 642°C, followed by $Mg_{12}Ce$, $Mg_6Zn_3Ca_2$, $Mg_{53}Zn_{45}Ce_2$, and MgZn phases formed at 511°C, 368°C, 333°C, and 294°C, respectively. Based on this and the diffusion simulation results [37], a new homogenization schedule, designated as H510 and shown in Figure 12(b), was designed with four isothermal stages (275°C for 4h, 375°C for 12h, 420°C for 2h, and 510°C for 1h) to sequentially dissolve each intermetallic phase without incipient melting. The first stage was chosen as 275°C between the formation temperatures of $Mg_{53}Zn_{45}Ce_2$ (333°C) and MgZn (294°C) in Figure 12(a) for 4 hours to firstly dissolve $Mg_{53}Zn_{45}Ce_2$ and MgZn phases. The second stage was designed as 375°C for 12 hours to reduce micro-segregation of alloying elements and further dissolve the second phases. A conventional homogenization profile (H390) was designed with one isothermal stage at 390°C for 48 hours, for comparison with the new homogenization profile (H510). Figure 13 shows that the new homogenization treatment (H510) is more effective

than the conventional homogenization treatment (H390) in dissolving the second phase particles from the as-cast Alloy 2.

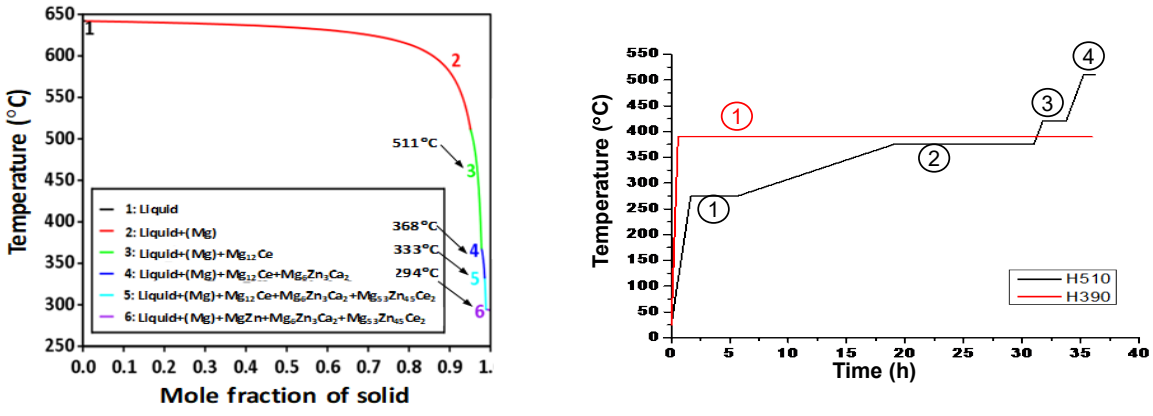

(a) (b)

Figure 12. (a) Calculated solidification path; and (b) Multi-stage homogenization profile (H510) and conventional homogenization profile (H390) designed for USAMP Alloy 2.

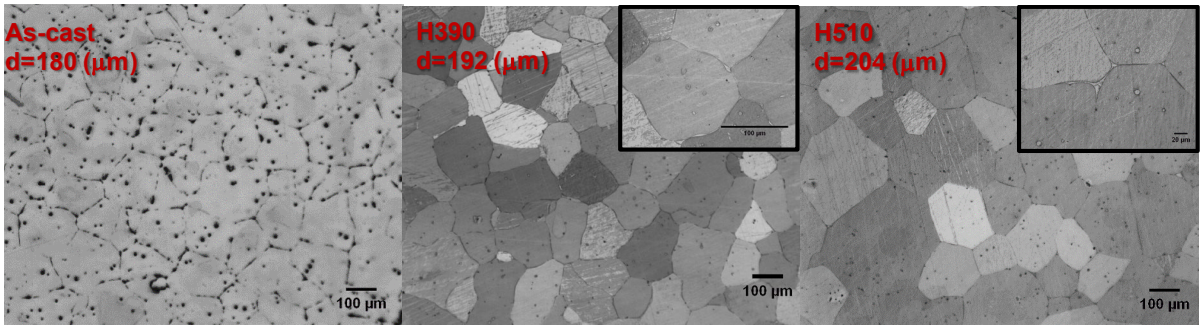

(a) As-cast (b) H390 (c) H510

Figure 13. Optical micrographs of USAMP Alloy 2: (a) as-cast condition; (b) after H390; and (c) after H510 homogenization treatments.

Figure 14 shows the tensile properties of Alloy 2 sheet with the two homogenization profiles followed by the same rolling and annealing process, and the results are also summarized in Table 4. The results show that the new homogenization profile (H510) produces excellent strength and ductility for Alloy 2. The Alloy 2 sheet samples in the as-rolled condition exhibit high yield strength (~269 MPa) and good elongation (~9.4%). Additionally, Alloy 2 sheet is heat-treatable, providing excellent elongation (~29%) and reasonable strength (157 MPa) after only 10 min of annealing from the as-rolled condition.

Table 4. Room-temperature tensile properties of USAMP Alloy 2 under different heat treatment conditions (reprinted from ref. 37 with permission).

Condition	Yield strength (MPa)	Ultimate tensile strength (MPa)	Elongation to failure (%)
H510-R400-AR	269±1	290±4	10±2.4
H510-R400-A350-10min	157±5	236±3	29±2.0
H390-R400-AR	223±4	253±6	8±3.0
H390-R400-A350-10min	148±3	228±3	22±3.3

Note that R400 denotes 400°C pre-heat prior to each rolling pass; A350 denotes annealing at 350°C; and AR denotes as-rolled condition.

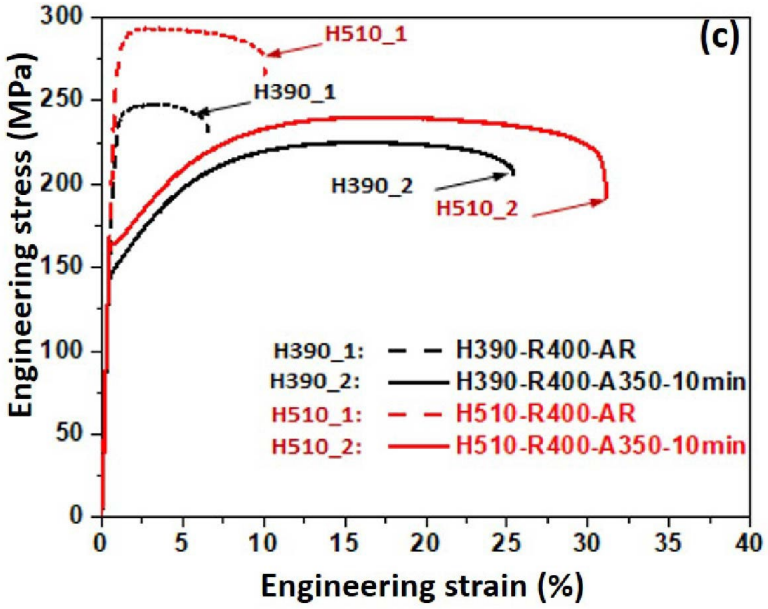

Figure 14. Tensile curves of ZXEM2000 alloy (Alloy 2) at room temperature (reprinted from ref. 37 with permission).

The electron backscatter diffraction (EBSD) inverse pole figure (IPF) map in Figure 15(a) shows the microstructure of Alloy 2 after rolling followed by annealing at 350°C for 10 minutes. Figure 15(b) shows a corresponding image quality map overlapped with large angle grain boundaries. The average grain size of Alloy 2 before rolling is about 126 μm as measured from EBSD. It is devident that the combination of rolling and annealing yields significant grain refinement in Alloy 2. The average grain size after annealing based on EBSD measurement is about 5.4 μm, which contributes to both high strength and high ductility. The texture pole figures of annealed microstructure are shown in Figure 15(c). The texture intensity is reduced, indicating a weak basal texture in the alloy has after annealing. The bright-field (BF) scanning transmission electron microscopy (STEM) image in Figure 15(d) shows a high density of evenly distributed Mn and $Mg_6Zn_3Ca_2$ precipitates in the annealed microstructure, also contributing to strengthening. Precipitates in annealed Alloy 2 specimens have similar morphology as those observed in as-rolled specimens. As shown in the enlarged view in Figure 15(d), some $Mg_6Zn_3Ca_2$ precipitates pin the grain boundaries. Such Zener pinning [38] may greatly reduce grain growth rates during annealing, thus resulting in fine grain sizes observed in Alloy 2.

In summary, the strength and ductility of Alloy 2 can be simultaneously improved with the new homogenization profile (H510). The new alloy sheet produced by rolling and annealing has an excellent combination of high ductility (29%) and good yield strength (157 MPa). Microstructure characterization shows that the following factors contribute to the above properties: (1) weak basal texture; (2) fine grain structure (average 5.4 μm); and (3) high density of evenly distributed and nano-sized Mn and $Mg_6Zn_3Ca_2$ precipitates.

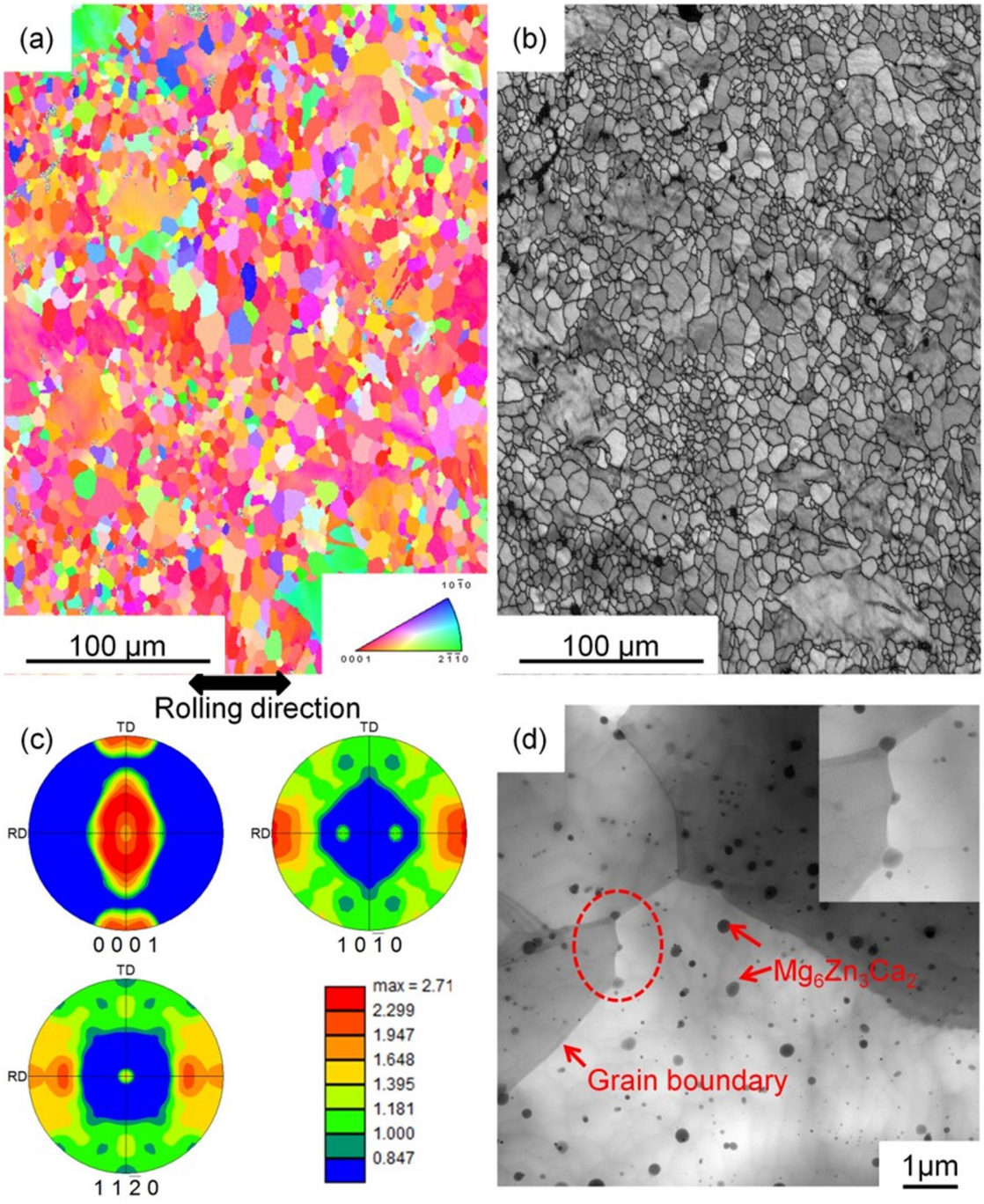

Figure 15. Characterization of the microstructure of ZXEM2000 (Alloy 2) after annealing at 350°C: (a) EBSD IPF map; (b) image quality map overlapped with grain boundaries with misorientation angles larger than 15° (black lines represent large angle grain boundaries); (c) texture pole figures; and (d) BF-STEM image with an enlarged view of the highlighted area in the circle, showing the Zener pinning effects of $Mg_6Zn_3Ca_2$ precipitate at grain boundaries (reprinted from ref. 37 with permission).

ZAXME11100 (USAMP Alloy 2 Plus)

Although Alloy 2 shows greater ductility than AZ31B alloy, it has similar room-temperature (RT) formability, Index Erichsen (I.E.) value of 6.5 mm (using a 20 mm diameter hemispherical punch on 1 mm sheet samples), as ZEK100 (6.7 mm) and E-Form Plus (6.2 mm) alloys. ZAXME11100 (USAMP Alloy 2 Plus), Mg-1.0Zn-1.0Al-0.5Ca-0.4Mn-0.2Ce, was designed to further improve its RT formability and age-hardening response

[39]. From Alloy 2 to Alloy 2 Plus, 2% Zn was replaced by 1% Zn and 1%Al, and Mn content was increased from 0.1% to 0.4%. The reason for introducing Al and increasing Mn content is highlighted in Figure 10, which shows that the Al-Mn atomic pair has the strongest affinity and could form crystalline Al_8Mn_5 phase. Other atomic pairs with negative mixing enthalpies may form some clusters [18, 40] without forming crystalline precipitates during aging treatment.

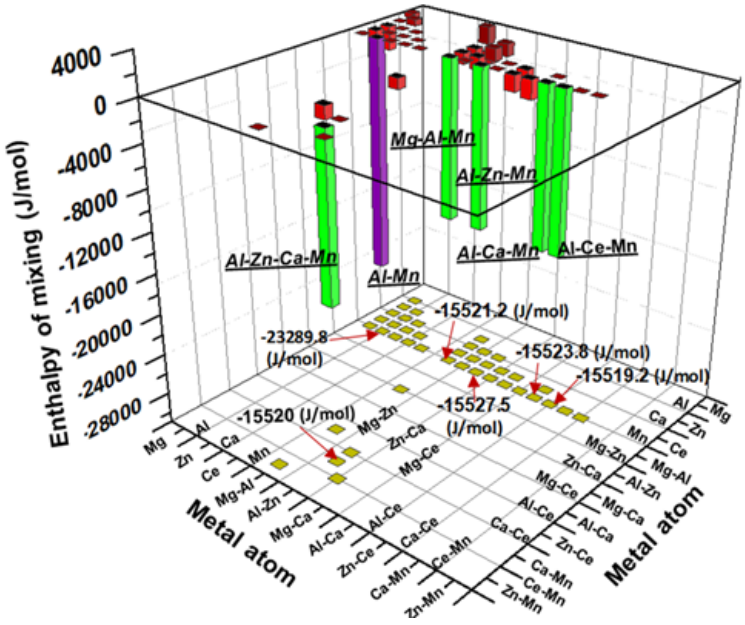

Figure 16. Projection of mixing enthalpy of various equiatomic pairs in Mg (hcp) matrix (reprinted from ref. 39, under the terms of the Creative Commons CC BY license).

Figure 17(a) is calculated solidification path of Alloy 2 Plus using the Scheil model, and an enlarged region near the end of solidification is shown in Figure 17(b). The results show that primary Mg phase will form at 638°C, followed by Al_8Mn_5, $Mg_{12}Ce$, Al_2Ca, $Ca_2Mg_5Zn_5$, $Ce_2Mg_{53}Zn_{45}$, $Al_{11}Mn_4$ and $Ca_2Mg_5Zn_{13}$ phases formed at 628°C, 546°C, 488°C, 368°C, 357°C, 329°C and 325°C, respectively. Figure 17(c) is the equilibrium phase fraction vs. temperature plot for Alloy 2 Plus, and the solidus temperature of Alloy 2 Plus is calculated to be 450°C. The calculated formation temperatures of Al_8Mn_5 and $Mg_{12}Ce$ are 632°C and 548°C, respectively, in Figure 17(c), which are slightly higher than those (628°C and 546°C, respectively) of the same phases during cooling (solidification) in Figures 17(a) and (b). Similarly, the formation of Al_2Ca, $Ca_2Mg_5Zn_5$ and $Al_{11}Mn_4$ is at 430°C, 172°C, and 208°C, respectively, which is considerably lower than their formation temperatures (488°C, 368°C, and 329°C) during solidification in Figures 17(a) and (b). Finally, $Ce_2Mg_{53}Zn_{45}$ and $Ca_2Mg_5Zn_{13}$ phases formed during solidification in Figure 17(b) are not shown in the equilibrium calculation in Figure 11(c), thus they are likely metastable phases.

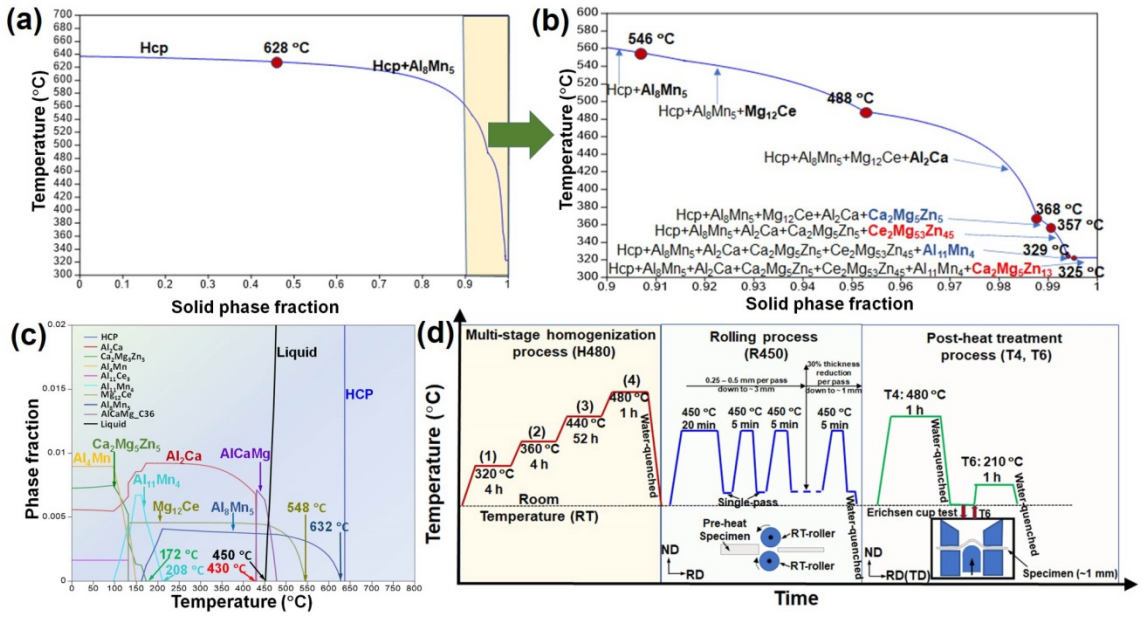

Figure 17. (a) Calculated solidification path; (b) The enlarged solidification path from the selection in Figure 1(a); (c) equilibrium phase fraction vs. temperature calculations; and (d) thermomechanical processes for producing ZAXME11100 (Alloy 2 Plus) sheet alloy (reprinted from ref. 39, under the terms of the Creative Commons CC BY license).

Similar to H510 for Alloy 2, a new homogenization profile (designated as H480) was designed with four isothermal stages (320°C for 4 h, 360°C for 4 h, 440°C for 52 h and 480°C for 1 h) to sequentially dissolve the intermetallic phases without incipient melting. The first stage was set at 320°C to dissovle $Ca_2Mg_5Zn_5$ and $Al_{11}Mn_4$ phases with the lowested formation temepratures (172°C and 208°C, respectively) in Figure 17(c). The second stage was designed at 360°C for 4 h to further dissolve the phases with higher melting temperatures, such as $Ca_2Mg_5Zn_5$ phase (368°C) in Figure 17(b) and also reduce the micro-segregation of alloying elements. The third stage was conducted at 440°C for 52 h, slightly above the formation temperature of Al_2Ca (430°C) in Figure 17(c) and (488°C) in Figure 11(b), to dissolve Al_2Ca phase and further homogenize the alloying elements. Figure 17(c) shows a small fraction of liquid at temperatures above the solidus 450°C. According to the modeling results in Figure 17(c), a new phase AlCaMg was possible to form during this stage since it is thermodynamically stable between 430°C and 478°C. Thus, the fourth stage was added at 480°C for 1 h to dissolve AlCaMg and potentially $Mg_{12}Ce$ and Al_8Mn_5 phases with higher thermal stability up to 548°C and 632°C, respectively.

Figure 18(a) shows the calculated solute distributions of solutes Al, Zn, Ca, Ce and Mn in Mg matrix in both the as-cast (AC) condition and the new H480-homogenized condition, based on diffusion simulation using DICTRA. The results suggest that the new multi-stage treatment is very effective in dissolving solute elements in Mg grain structure. The diffusion coefficients (of Al, Zn, Ca, Mn and Ce solutes in Alloy 2) vs. temperature in Figure 18(b) show an exponential relationship. For example, the diffusion coefficients of the solutes at 480°C are about 10 times higher than those at 400°C, indicating significantly faster homogenization at 480°C compared to 400°C (which is below the 450°C solidus). Specifically, Al and Mn have the lowest diffusion coefficients among all alloying elements in Mg, which explains why Al_8Mn_5 is the most difficult phase to be dissolved during solution treatment. Figures 18(c) and (d) show optical microscophs of Alloy 2 Plus in the as-cast condition and

after multi-stage homogenization treatment (H480), respectively. It can be seen that the second phase particles near and along the grain boundaries are essentially dissolved after the new homogenization profile (H480). However, a small amount of residual particles, mostly Al_8Mn_5 and a very few Al_2Ca as identified by TEM, are still visible in Figure 18(d).

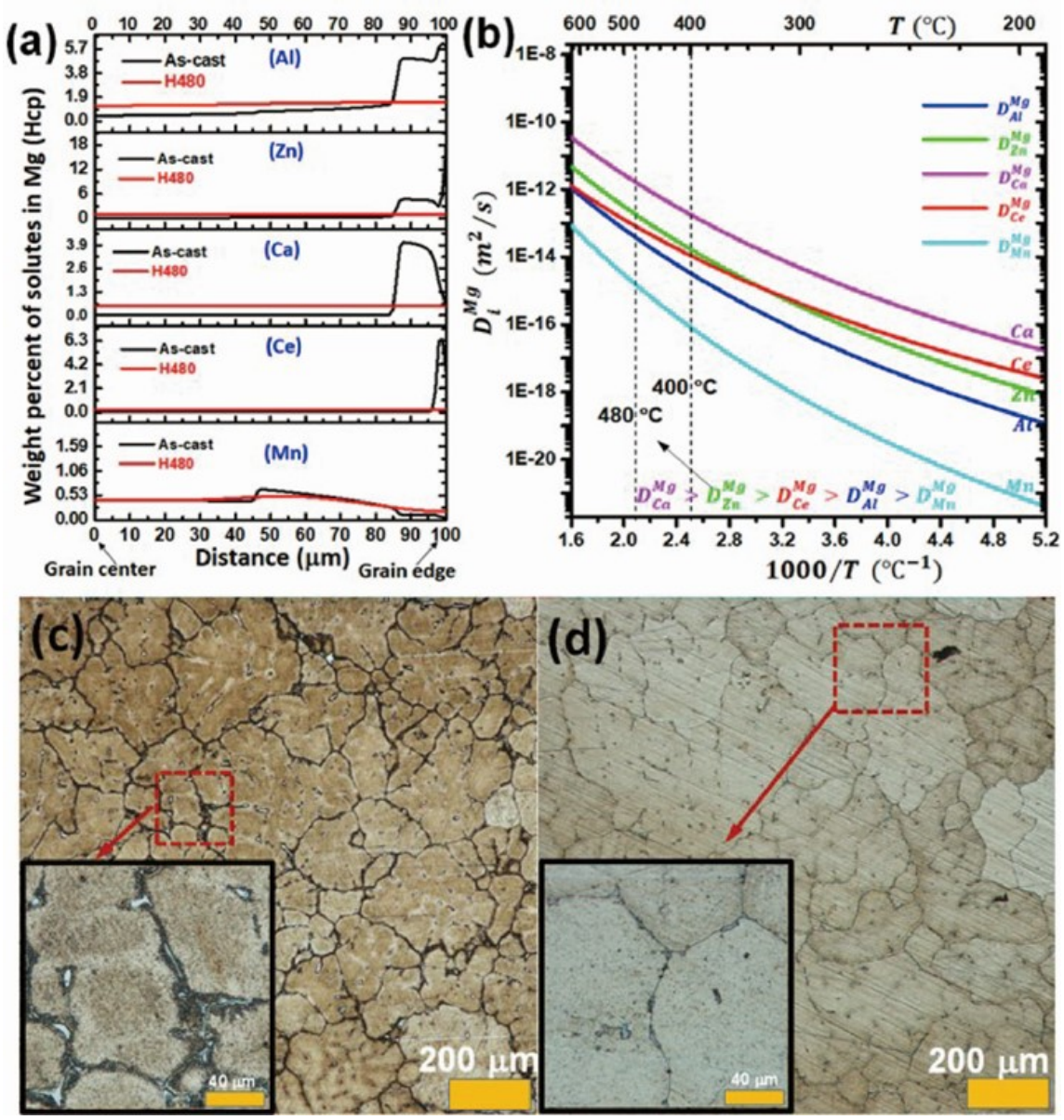

Figure 18. (a) Diffusion modeling results of Al, Zn, Ca, Ce and Mn solutes in Mg (hcp); (b) solute diffusion coefficients in Mg (hcp); optical micrographs of (c) as-cast condition; and (d) after H480 homogenization ZAXME11100 (Alloy 2 Plus) (reprinted from ref. 39, under the terms of the Creative Commons CC BY license).

Figure 19(a) shows the microstructure of Alloy 2 Plus after rolling process (R450) followed by a post-forming solution treatment (T4) and water quenching from Figure 17(d). The average grain size of Alloy 2 Plus determined via EBSD is about 9.6 μm. It is clear that the combination of rolling (R450) and post-forming solution-treatment (T4) leads to significant grain refinement in the alloy. The pole figure results of solution-treated (T4) microstructure in Figure 19(b) show a weak split basal texture with a maximum intensity of 3.3 mrd. The

maximum intensity of basal poles is tilted by about ±40 degrees away from the normal direction (ND) and toward the transverse direction (TD). Such fine grain size and weak texture of the solution-treated (T4) Alloy 2 Plus sheet contribute to high ductility and formability.

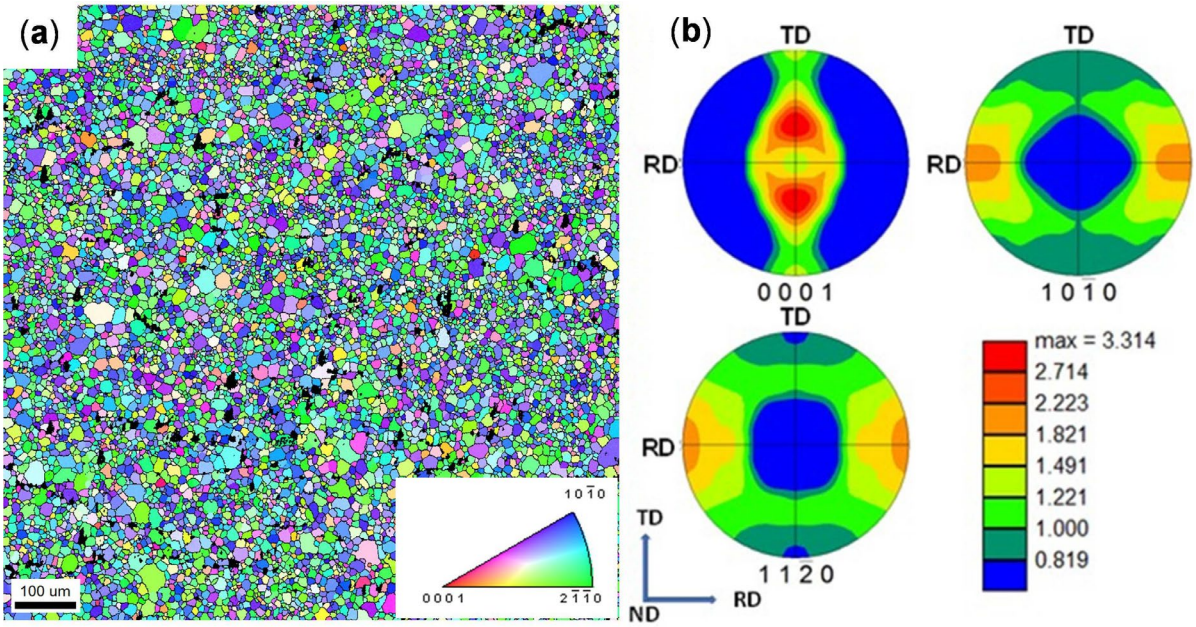

Figure 19. EBSD microstructure of ZAXME11100 (Alloy 2 Plus) after solution-treated (T4) at 480°C for 1 hour: (a) EBSD IPF map; (b) texture pole figures (reprinted from ref. 39, under the terms of the Creative Commons CC BY license).

Figure 20 compares Erichsen cup test results of the most formable magnesium sheet alloys at room temperature, with Alloy 2 Plus showing the highest formability, i.e., Index Erichsen (I.E.) value of 7.8 mm compared to 6.5 mm for Alloy 2. Figure 21(a) shows the age hardening curve of solution-treated (T4) Alloy 2 Plus sheet alloy at 210°C. Alloy 2 Plus sheet has a hardness value of 56.0 ± 2.1 HV in the solution treated condition (T4) from Figure 17(d) and shows a rapid aging response to a peak hardness of 70.8 ± 1.5 HV (about 26% increase) in only 1 hour. Figure 21(b) dispalys the tensile stress vs. strain results tested from the solution-treated (T4) and peak-aged (T6) samples. The tensile properties of these samples are also listed in Table 5. The T4 treated Alloy 2 Plus sheet offers a decent yield strength (Y.S.) of 159 MPa and an UTS (ultimate tensile strength) of 253 MPa with an exceptionally high elongation of 31%.

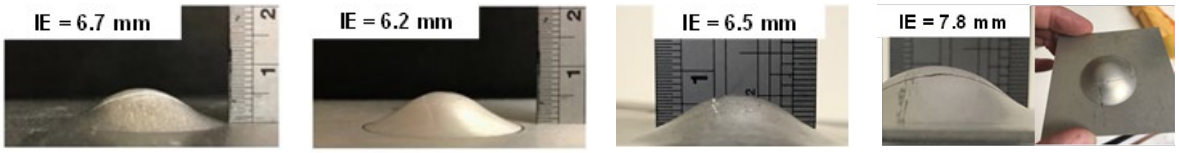

(a) ZEK100 (b) E-Form Plus (c) USAMP Alloy 2 (d) USAMP Alloy 2 Plus

Figure 20. Formability (Erichsen test results) of various magnesium alloys at room temperature: (a) ZEK100; (b) E-Form Plus; (c) USAMP Alloy 2; and (d) USAMP Alloy 2 Plus (courtesy of T.D. Berman, J.E. Allison [41]).

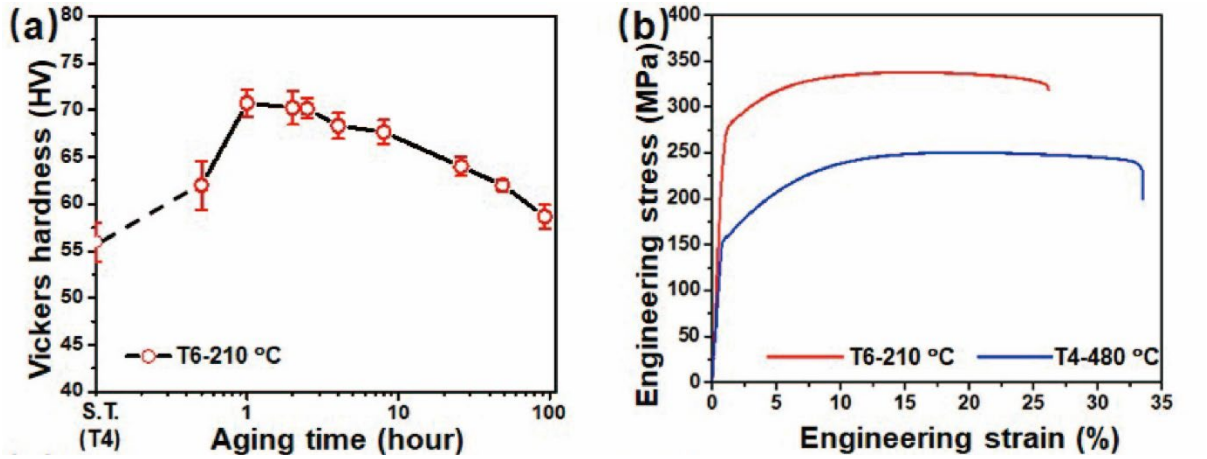

Figure 21. (a) Age hardening response at 210°C; and (b) tensile curves from the T4 and peak-aged T6 treated ZAXME11100 alloy (Alloy 2 Plus) samples (reprinted from ref. 39, under the terms of the Creative Commons CC BY license).

Table 5. Mechanical properties of ZAXME11100 (Alloy 2 Plus) sheet alloy at room temperature (reprinted from ref. 39, under the terms of the Creative Commons CC BY license).

Temper	Y.S. (MPa)	U.T.S. (MPa)	Elongation (%)	I.E. (mm)
T4-480°C, 1 h	159.2±2.5	252.6±2.3	30.5±3.1	7.8±0.1
T6-210°C, 1 h	270.3±0.4	332.4±5.3	25.8±1.8	N/A

After a short aging treatment (T6), the yield strength and UTS of Alloy 2 Plus have been greatly improved to 270 MPa and 332 MPa, respectively, and yet a high elongation of 26%. It is clear that the Alloy 2 Plus sheet provides excellent formability in T4 condition, which is similar to that of 6000 series Al alloys (7.6 mm for 6061-O [42] and ~10 mm for 6016-T4 [43]). Following T4, an artificial aging (T6) can significantly increase the yield strength with only a slight reduction in ductility, offering a well-balanced high strength, ductility and formability at room temperature. It should be pointed out that a post-forming T6 treatment (~1 h at 210°C) can be achieved or adjusted to the automotive body paint bake process used for the sheet components.

Figures 22(a) and (b) show STEM imaging for the T6 microstructure of Alloy 2 Plus, where no visible crystalline precipitate phases were found, except for the nano-size Al_8Mn_5 rods which already existed in the solution-treated samples [39]. This again indicates that Al and Mn solutes have the strongest affinity in Alloy 2 Plus to potentially form crystalline phases during aging. No Guinier Preston (G.P.) zones or metastable phases were observed in the STEM or HAADF-STEM images in Figure 22. Figure 16 shows the enthalpy of mixing values of various atomic pairs in Mg matrix, suggesting the most negative enthalpy of mixing for the Al-Mn pair (-23289.8 J/mol). Although the Al-Mn pair is thermodynamically favored to form crystalline phases during aging, no visible precipitates were observed in the microstructure, Figure 22(b). Therefore, it is speculated that the significant enhancement of yield strength and UTS after T6 treatment is due to the formation of solute clusters as shown in Figure 22(c), with a pinning effect on the basal <a> dislocations. It was also reported [40] that co-clustering of Al, Zn and Ca atoms can provide age-hardening in a Mg-1.3Al-0.8Zn-0.7Mn-0.5Ca alloy. Research is ongoing to identify and characterize solute clusters in Alloy 2 Plus, using advanced Atom Probe Tomography (APT) technique.

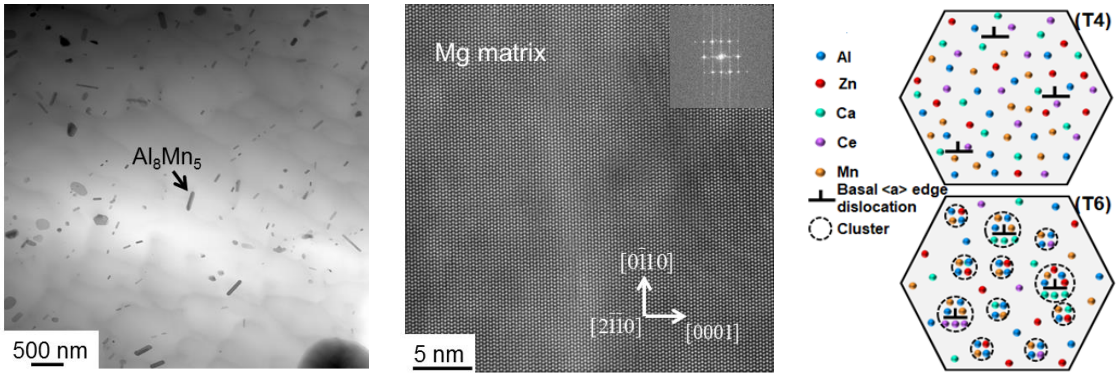

(a) (b) (c)

Figure 22. Microstructure of ZAXME11100 (Alloy 2 Plus) after aging treatment (T6) at 210°C for 1 hour: (a) bright field STEM image; (b) atomic resolution HAADF-STEM image; and (c) top-T4: solute atoms dissolve into Mg (hcp) after solution treatment and bottom-T6: solute atoms not only segregate to basal <a> dislocations but also form small clusters during a short aging time (reprinted from ref. 39, under the terms of the Creative Commons CC BY license).

SUMMARY AND FUTURE OUTLOOK

Figure 23 plots Index Erichsen value vs. yield strength at RT for AZ31 [34] and various alloys evaluated in the USAMP project. Compared to commercial AZ31B alloy, ZEK100, E-Form Plus and USAMP Alloy 2 all show improved room-temperature formability, but with slightly reduced yield strength. The new sheet alloy, ZAXME11100 (USAMP Alloy 2 Plus), offers both excellent ductility (31% tensile elongation) and RT formability (7.8 mm Erichsen Index) in the solution-treated condition (T4), but with an extraordinary high yield strength (270 MPa) upon post-forming aging treatment (T6). Table 6 compares the room temperature mechanical properties and formability of magnesium sheet alloys with aluminum alloys 6061 [42] and 6016 [43]. The excellent combination of strength and formability of this new magnesium alloy, comparable to those of 6000 sheet aluminum alloys (AA6016 and AA6061), clearly shows potential for room temperature forming of automotive applications.

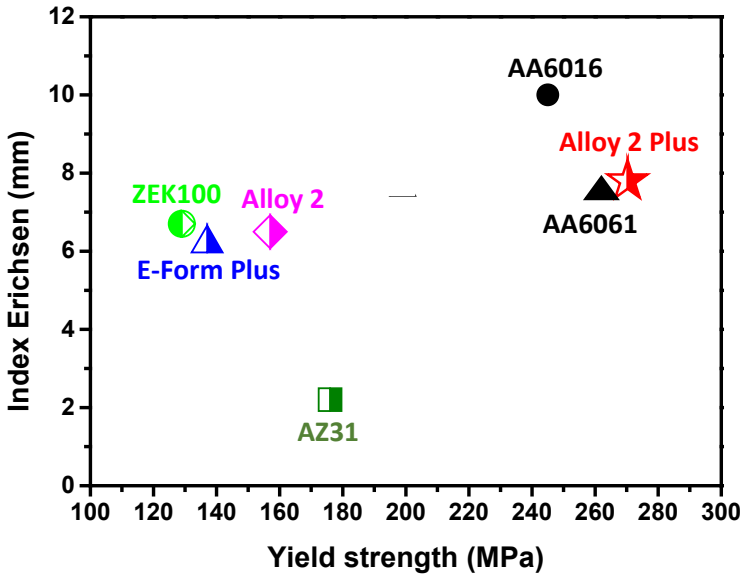

Figure 23. RT formability (Index Erichsen values [41]) vs. yield strength of various new magnesium alloys evaluated by USAMP, in comparison with commercial magnesium alloy AZ31B [34] and aluminum alloys 6061 [42] and 6016 [43]. For age-hardening Alloy 2 Plus, AA6061 and AA6016 alloy, the EI was measured at T4 temper, while the yield strength is tested at T6 conditions.

Table 6. Room temperature mechanical properties and formability of magnesium sheet alloys compared to aluminum alloys 6061 [42] and 6016 [43]

Family: Alloy-Temper	Y.S. (MPa)	U.T.S. (MPa)	Elongation (%)	I.E. (mm)
Mg: AZ31	170	260	17	2.2
Mg: ZEK100 O	130	250	25	6.7
Mg: E-form Plus	150	250	22	6.2
Mg: Alloy 2 Plus T4 (480 °C, 1 h)	159	253	31	7.8
Mg: Alloy 2 Plus T6 (210 °C, 1 h)	270	332	26	N/A
Al: 6061 T4 (550 ℃, 2 h)	*63*	*185*	*16*	*7.6*
Al: 6061 T6 (200 ℃, 2 h)	*260*	*314*	*9*	*6.8*
Al: 6016 T4 (560 ℃)	*109*	*230*	*26*	*10.6*
Al: 6016 T6 (180 ℃, 2 h)	*240*	*N/A*	*N/A*	*N/A*

Magnesium sheet alloy development and evulation efforts in the last 20 years have generated critical new understanding of room-temperature formability of magnesium alloys. These research efforts have highlighted the potential avenues for improving RT formability of magnesium alloys:

1) Texture modification. It has been shown in this paper that the RT formability is greatly improved when the texture intensity is reduced, especially via alloying elements in magnesium solid solution. Rare earth elements (such as Ce) as well as Ca have been found effective in reducing texture intensity. It is also critically important to dissolve these alloying elements in magnesium solution, multi-stage homoenization to sequentially dissolve various phases can be designed based on CALPHAD modeling.
2) Grain structure. It is clear from this paper and literature that unformly fine grain structure can benefit the strength, ductility and RT formability of magnesium alloys. This can be achieved through alloy design (such as adding grain-refiners), casting (fast cooling rates) and subsequent TMP processing (promoting dynamic recrystallization).

ACKNOWLEDGEMENTS

The authors acknowledge Tracy Berman and John Allison of University of Michigan for conducting Erichsen cupping test, Randy Gerken of FiatChrysler, Anil Sachdev and Jon Carter of General Motors, Bita Ghaffari of Ford Motor Company and the entire USAMP project team for many helpful discussions.

This work is partially supported by the United States Automotive Materials Partnership (USAMP) and by the U.S. Department of Energy (DOE) National Energy Technology Laboratory under Award Number DE-EE0007756. This report was prepared as an account of work sponsored by an agency of the United States Government. Neither the United States Government nor any agency thereof, nor any of their employees, makes any warranty, express or implied, or assumes any legal liability or responsibility for the accuracy, completeness, or usefulness of any information, apparatus, product, or process disclosed, or represents that its use would not infringe privately owned rights. Reference herein to any specific commercial product, process, or service by trade name, trademark, manufacturer, or otherwise does not necessarily constitute or imply its endorsement, recommendation, or favoring by the United States Government or any agency thereof. The views and opinions of authors expressed herein do not necessarily state or reflect those of the United States Government or any agency thereof.

Conflicts of interest statement

On behalf of all authors, the corresponding author states that there is no conflict of interest.

References

1. W.J. Joost, P.E. Krajewski, *Scripta Materialia,* 128, 107 (2017).
2. A. Taub, E. De Moor, A. Luo, D.K. Matlock, J.G. Speer, U. Vaidya, *Annual Review of Materials Research*, 49, 327 (2019).
3. A.A. Luo, *Magnesium: The Lightest Structural Metal*, (Saint Paul, MN: International Magnesium Association, 2018), pp. 1-47.
4. B.R. Powell, A.A. Luo, P.E. Krajewski, *Advanced Materials in Automotive Engineering*, (Cambridge, UK: Woodhead Publishing Ltd, 2012), pp. 150-209.
5. A.A. Luo, *Journal of Magnesium and Alloys*, 1, 2 (2013).
6. A.A. Luo, *SAE International Journal of Materials and Manufacturing*, 114, 411 (2005).
7. A.A. Luo, R.C. McCune, "Magnesium Front End — AMD 603 and AMD 604", *Automotive Lightweighting Materials*, (Washington DC: The United States Department of Energy FY 2006 Progress Report*,* 2007).
8. A.A. Luo, J.F. Quinn, Y.-M. Wang, T.M. Lee, R. Verma, D.A. Wagner, J.H. Forsmark, X. Su, J. Zindel, M. Li, S.D. Logan, S. Bilkhu, R.C. McCune, *Light Metal Age*, (2), 54 (2012).
9. J. Forsmark, M. Li, X. Su, D. Wagner, J. Zindel, A. Luo, J. Quinn, R. Verma, Y. Wang, S. Logan, S. Bilkhu, R. McCune, *Magnesium Technology 2014*, Eds. M. Alderman, M.V. Manuel, N. Hort, and N.R. Neelameggham, (Warrendale, PA: TMS, 2014), p. 517.
10. P.E. Krajewski, 'Warm Forming of Aluminum: Summary of USAMP Project AMD307', presentation at *Materials Science & Technology Conference*, (Cincinnati, OH: Oct. 15, 2006).
11. P. Friedman, 'Development of High-Volume Warm Forming of Low-Cost Magnesium Sheet Project', presentation at *DOE Annual Merit Revie Meeting*, (Washington, DC: June 7-11, 2010).
12. POSCO, *Magnesium Sheet*, (Pohang, South Korea: POSCO, 2018), pp. 380-381.
13. D.A. Wagner, S.D. Logan, K. Wang, T. Skszek, *Magnesium Technology 2010*, Eds. S.R. Agnew, N.R. Neelameggham, E.A. Nyberg, W.H. Sillekens (Warrendale, PA: TMS, 2010), p 547.
14. D. Wagner, S. Logan, K. Wang, T. Skszek, *SAE Technical Paper 2010-01-0405*, (2010) https://doi.org/10.4271/2010-01-0405.
15. Y. Chino, K. Sassa, M. Mabuchi, *Mat. Sci. Eng.: A*, 513-514, 394 (2009).
16. T.T.T. Trang, J.H. Zhang, J.H. Kim, A. Zargaran, J.H. Hwang, B.-C. Suh and N.J. Kim, *Nat. Commun.*, 9, 2522 (2018).
17. Y. Chino, K. Sassa, M. Mabuchi, *Mater. Trans.*, 49, 1710 (2008).
18. M.Z. Bian, T.T. Sasaki, T. Nakata, S. Kamado, K. Hono, *Mat. Sci. Eng.*: *A*, 730, 147 (2018).
19. Y. Chino, K. Sassa and M. Mabuchi, *Mater. Trans.*, 49, 2916 (2008).
20. A.A. Luo, R.K. Mishra and A.K. Sachdev, *Scr. Mater.*, 64, 410 (2011).

21. T.T. Sasaki, F.R. Elsayed, T. Nakata, T. Ohkubo, S. Kamado, K. Hono, *Acta Mater.* 99, 176 (2015).
22. Z.R. Zeng, Y.M. Zhu, R.L. Liu, S.W. Xu, C.H.J. Davies, J.F. Nie, N. Birbilis, *Acta Mater.*, 160, 97 (2018).
23. M.Z. Bian, T.T. Sasaki, B.C. Suh, T. Nakata, S. Kamado, K. Hono, *Scr. Mater.*, 138, 151 (2017).
24. S.W. Xu, K. Oh-ishi, S. Kamado, F. Uchida, T. Homma, K. Hono, *Scr. Mater.*, 65, 269 (2011).
25. Z.R. Zeng, Y.M. Zhu, S.W. Xu, M.Z. Bian, C.H.J. Davies, N. Birbilis, J.F. Nie, *Acta Mater.*, 105, 479 (2016).
26. B.P. Zhang, L. Geng, L.J. Huang, X.X. Zhang, and C.C. Dong, *Scr. Mater.*, 63, 1024 (2010).
27. J.D. Robson, D.T. Henry, B. Davis, *Acta Mater.*, 57, 2739 (2009).
28. S. Sandlöbes, M. Friák, S. Zaefferer, A. Dick, S. Yi, D. Letzig, Z. Pei, L.-F. Zhu, J. Neugebauer, D. Raabe, *Acta Mater.*, 60, 3011 (2012).
29. G. Liu, J. Zhang, G. Xi, R. Zuo, S. Liu, *Acta Mater.*, 141, 1 (2017).
30. A.A. Luo, *CALPHAD,* 50, 6 (2015).
31. R. Shi, A.A. Luo, *CALPHAD*, 62, 1 (2018).
32. Luxfer Magnesium Rolled Products, *Elektron 717*, https://luxferga.com/app/uploads/Luxfer-Elektron-717_2018.pdf.
33. W. Muhammad, M. Mohammadi, J. Kang, R.K. Mishra, K. Inal, *International Journal of Plasticity*, 70 30 (2015).
34. U.M. Chaudry, T.H. Kim, S.D. Park, Y.S. Kim, K. Hamad, J.-G. Kim, *Materials*, 11, 2201 (2018).
35. W. Bang, J.K. Kim, 'Case studies: recent electronics application development with POSCO magnesium flat products', presentation at *IMA World Magnesium Conference*, (New Orleans, LA: May 16-18, 2018).
36. U.M. Chaudry, T.H. Kim, S.D. Park, Y.S. Kim, K. Hamad, J.-G. Kim, *Mater. Sci. Eng. A*, 739, 289 (2019).
37. R. Shi, J. Miao, A.A. Luo, *Scr. Mater.*, 171, 92 (2019).
38. R.J. Perez, H.G. Jiang, C.P. Dogan, E.J. Lavernia, *Metall. Mater. Trans. A,* 29A, 2469 (1988).
39. R. Shi, J. Miao, T. Avey, A.A. Luo, *Scientific Reports*, 10, (1), 1 (2020).
40. M.Z. Bian, T.T. Sasaki, T. Nakata, Y. Yoshida, N. Kawabe, S. Kamado, K. Hono, *Acta Mater.* 158, 278 (2018).
41. T.D. Berman, J.E. Allison, University of Michigan, Ann Arbor, MI, unpublished research, 2020.
42. F. Ozturk, E. Esener, S. Toros, C.R. Picu, *Mater. Des.* 31, 4847 (2010)
43. S.M. Hirth, G.J. Marshall, S.A. Court, D.J. Lloyd, *Mater. Sci. Eng. A.*, 452, 319–321 (2001).